



Contents lists available at ScienceDirect

Journal of Quantitative Spectroscopy & Radiative Transfer

journal homepage: www.elsevier.com/locate/jqsrt

Coupled-dipole method for magnetic and negative-refraction materials

Patrick C. Chaumet^{a,*}, Adel Rahmani^b^a Institut Fresnel (UMR 6133), Université Paul Cézanne, Avenue Escadrille Normandie-Niemen, F-13397 Marseille cedex 20, France^b Department of Mathematical Sciences and Centre for Ultrahigh-bandwidth Devices for Optical Systems, University of Technology, Sydney, Broadway NSW 2007, Australia

ARTICLE INFO

Article history:

Received 19 June 2008

Received in revised form

3 September 2008

Accepted 3 September 2008

ABSTRACT

We present a derivation of the coupled-dipole method, also called discrete dipole approximation, for scatterers with arbitrary dielectric permittivity and magnetic permeability. We discuss the numerical implementation of the method and illustrate its application to magnetic and negative-refraction materials.

© 2008 Elsevier Ltd. All rights reserved.

1. Introduction

The coupled-dipole method (CDM), also called discrete dipole approximation or DDA, is widely used to study the scattering of light by single particles, or clusters of particles of arbitrary shapes [1–11]. A recent review on this method is given in [12]. In the CDM, arbitrary scatterers are discretized over a spatial grid and represented as a collection of electric dipoles. The electromagnetic fields are first derived self-consistently inside the scatterer. The fields anywhere outside the scatterer can be computed by propagating the internal fields using an appropriate field-susceptibility tensor.

Beyond the standard problem of the scattering of light by a dielectric particle, the method has been successfully used to study a number of other problems in electrodynamics, including spontaneous emission near a structured substrate [4], Purcell effect in microcavities [13,14], optical forces and torques [15–17], optical binding [18], near-field optical nanomanipulation [19,20], optical trapping near a photonic crystal cavity [21], plasmon enhanced Raman scattering [22], optical tomography [23], and light scattering by particles larger than the wavelength [24,25].

Traditionally, the CDM has been used to study light scattering problems involving non-magnetic materials. In the past, magnetic dipole terms have generally been introduced as a means of improving the convergence of the method for large dielectric particles, rather than to describe materials with magnetic properties [26,27]. However, Lakhtakia considered a non-trivial magnetic permeability in his treatment of bianisotropic scatterers [28] and recently, You et al. presented a derivation of the DDA with a magnetic permeability different from one to study the electromagnetic cloaking properties of coated spheres [29]. However, no study of the convergence of the CDM for magnetic and negative-refraction materials has been performed yet.

In this paper, we present a detailed derivation of the CDM for materials with arbitrary dielectric permittivity and magnetic permeability based on the field-susceptibility tensors associated to the electromagnetic fields. We consider different prescriptions of the polarizabilities, including the one resulting from a rigorous integration of the field-susceptibility tensors over the discretization cells. This means that our formulation takes into account the variations of the

* Corresponding author.

E-mail address: patrick.chaumet@fresnel.fr (P.C. Chaumet).

tensors across each cells which, as we showed in [3], is instrumental in improving the performance of the DDA for scatterers with a large refractive index. We compare our cross-section calculations to the rigorous Mie theory in the case of spherical scatterers; in particular we examine the convergence of the CDM for magnetic and negative-refraction materials.

2. CDM for magnetic and electric medium

We first start by deriving the self-consistent electric and magnetic field in terms of the electric and magnetic properties of the scatterer.

From Maxwell's equations in CGS unit, we can write [30]

$$(\nabla^2 + k_0^2)\mathbf{E}_m = -4\pi[k_0^2\mathbf{P} + \nabla(\nabla \cdot \mathbf{P})] - 4\pi ik_0 \nabla \times \mathbf{M} \quad (1)$$

$$(\nabla^2 + k_0^2)\mathbf{H}_m = -4\pi[k_0^2\mathbf{M} + \nabla(\nabla \cdot \mathbf{M})] + 4\pi ik_0 \nabla \times \mathbf{P} \quad (2)$$

where $\mathbf{P}(\mathbf{r}) = \chi^e(\mathbf{r})\mathbf{E}_m(\mathbf{r})$ is the polarization, $\mathbf{M}(\mathbf{r}) = \chi^m(\mathbf{r})\mathbf{H}_m(\mathbf{r})$ is the magnetization, and \mathbf{E}_m and \mathbf{H}_m are the macroscopic electric and magnetic fields. Consider a scatterer with relative permittivity tensor $\boldsymbol{\varepsilon}(\mathbf{r})$ and relative permeability tensor $\boldsymbol{\mu}(\mathbf{r})$, in vacuum, illuminated by an electromagnetic wave $\{\mathbf{E}_{\text{inc}}(\mathbf{r}), \mathbf{H}_{\text{inc}}(\mathbf{r})\}$. The electromagnetic field inside and outside the object can be expressed as

$$\mathbf{E}_m(\mathbf{r}) = \mathbf{E}_{\text{inc}}(\mathbf{r}) + \int_V \mathbf{G}^{ee}(\mathbf{r}, \mathbf{r}') \chi^e(\mathbf{r}') \mathbf{E}_m(\mathbf{r}') d\mathbf{r}' + \int_V \mathbf{G}^{em}(\mathbf{r}, \mathbf{r}') \chi^m(\mathbf{r}') \mathbf{H}_m(\mathbf{r}') d\mathbf{r}' \quad (3)$$

$$\mathbf{H}_m(\mathbf{r}) = \mathbf{H}_{\text{inc}}(\mathbf{r}) + \int_V \mathbf{G}^{me}(\mathbf{r}, \mathbf{r}') \chi^e(\mathbf{r}') \mathbf{E}_m(\mathbf{r}') d\mathbf{r}' + \int_V \mathbf{G}^{mm}(\mathbf{r}, \mathbf{r}') \chi^m(\mathbf{r}') \mathbf{H}_m(\mathbf{r}') d\mathbf{r}' \quad (4)$$

where V correspond to the volume of the object and the integrals are to be taken as principal values. The dyadic tensors \mathbf{G} are obtained by application of the appropriate differential operator to the free-space Green's function $G(\mathbf{r}, \mathbf{r}') = e^{ik_0|\mathbf{r}-\mathbf{r}'|}/|\mathbf{r}-\mathbf{r}'|$ associated to the source terms $\mathbf{P}(\mathbf{r}) = \mathbf{p}\delta(\mathbf{r}-\mathbf{r}')$ and $\mathbf{M}(\mathbf{r}) = \mathbf{m}\delta(\mathbf{r}-\mathbf{r}')$ [30]:

$$\mathbf{G}^{ee}(\mathbf{r}, \mathbf{r}')\mathbf{p} = [k_0^2\mathbf{p} + \nabla(\nabla \cdot \mathbf{p})]G(\mathbf{r}, \mathbf{r}') \quad (5)$$

$$\mathbf{G}^{em}(\mathbf{r}, \mathbf{r}')\mathbf{m} = [ik_0 \nabla \times \mathbf{m}]G(\mathbf{r}, \mathbf{r}') \quad (6)$$

$$\mathbf{G}^{me}(\mathbf{r}, \mathbf{r}')\mathbf{p} = [-ik_0 \nabla \times \mathbf{p}]G(\mathbf{r}, \mathbf{r}') \quad (7)$$

$$\mathbf{G}^{mm}(\mathbf{r}, \mathbf{r}')\mathbf{m} = [k_0^2\mathbf{m} + \nabla(\nabla \cdot \mathbf{m})]G(\mathbf{r}, \mathbf{r}') \quad (8)$$

These tensors represent the linear electric and magnetic susceptibilities associated with an electric or a magnetic dipole. Incidentally, one of the advantages of using CGS instead of MKSA units is that symmetry rules between electric and magnetic quantities are preserved, i.e. $\mathbf{G}^{ee} = \mathbf{G}^{mm}$ and $\mathbf{G}^{em} = -\mathbf{G}^{me}$. To solve Eqs. (3)–(4) the object is discretized into a set of N subunits arranged on a cubic lattice. If the subunits are small compared to the wavelength inside the object, one can assume that the linear electric (magnetic) susceptibility and the electric (magnetic) field are uniform over the subunit, then Eqs. (3)–(4) for the macroscopic field at subunit i inside the object can be written as

$$\mathbf{E}_m(\mathbf{r}_i) = \mathbf{E}_{\text{inc}}(\mathbf{r}_i) + \sum_{j=1}^N \int_{V_j} \mathbf{G}^{ee}(\mathbf{r}_i, \mathbf{r}') d\mathbf{r}' \chi^e(\mathbf{r}_j) \mathbf{E}_m(\mathbf{r}_j) + \sum_{j=1}^N \int_{V_j} \mathbf{G}^{em}(\mathbf{r}_i, \mathbf{r}') d\mathbf{r}' \chi^m(\mathbf{r}_j) \mathbf{H}_m(\mathbf{r}_j) \quad (9)$$

$$\mathbf{H}_m(\mathbf{r}_i) = \mathbf{H}_{\text{inc}}(\mathbf{r}_i) + \sum_{j=1}^N \int_{V_j} \mathbf{G}^{me}(\mathbf{r}_i, \mathbf{r}') d\mathbf{r}' \chi^e(\mathbf{r}_j) \mathbf{E}_m(\mathbf{r}_j) + \sum_{j=1}^N \int_{V_j} \mathbf{G}^{mm}(\mathbf{r}_i, \mathbf{r}') d\mathbf{r}' \chi^m(\mathbf{r}_j) \mathbf{H}_m(\mathbf{r}_j) \quad (10)$$

We will use the notation $\mathbf{G}_{\text{int}}(\mathbf{r}_i, \mathbf{r}_j) = \int_{V_j} \mathbf{G}(\mathbf{r}_i, \mathbf{r}') d\mathbf{r}'$. When $i \neq j$ the integration can be done directly whereas when $i = j$ (interaction of the subunit with itself) the integral must be rewritten in a form more suitable to numerical integration. In Ref. [3] we presented a detailed derivation of the exact form of $\int_{V_i} \mathbf{G}^{ee}(\mathbf{r}_i, \mathbf{r}') d\mathbf{r}'$, however, many approximation of this term have been used in the past [2,29,31–33]. It is obvious that $\int_{V_i} \mathbf{G}^{mm}(\mathbf{r}_i, \mathbf{r}') d\mathbf{r}' = \int_{V_i} \mathbf{G}^{ee}(\mathbf{r}_i, \mathbf{r}') d\mathbf{r}'$ since the two field-susceptibility tensors are identical. Regarding the mixed terms, i.e. \mathbf{G}^{em} and \mathbf{G}^{me} , from the parity of the tensors it follows that

$$\int_{V_i} \mathbf{G}^{em}(\mathbf{r}_i, \mathbf{r}') d\mathbf{r}' = \int_{V_i} \mathbf{G}^{me}(\mathbf{r}_i, \mathbf{r}') d\mathbf{r}' = \mathbf{0} \quad (11)$$

At this stage we can rewrite Eqs. (9)–(10) in terms of the local fields (\mathbf{E} and \mathbf{H}), i.e. the fields at a given subunit in the absence of the subunit:

$$\mathbf{E}(\mathbf{r}_i) = \mathbf{E}_{\text{inc}}(\mathbf{r}_i) + \sum_{j=1}^N [\mathbf{G}_{\text{int}}^{ee}(\mathbf{r}_i, \mathbf{r}_j) \boldsymbol{\alpha}^e(\mathbf{r}_j) \mathbf{E}(\mathbf{r}_j) + \mathbf{G}_{\text{int}}^{em}(\mathbf{r}_i, \mathbf{r}_j) \boldsymbol{\alpha}^m(\mathbf{r}_j) \mathbf{H}(\mathbf{r}_j)] \quad (12)$$

$$\mathbf{H}(\mathbf{r}_i) = \mathbf{H}_{\text{inc}}(\mathbf{r}_i) + \sum_{j=1}^N{}' [\mathbf{G}_{\text{int}}^{\text{me}}(\mathbf{r}_i, \mathbf{r}_j) \boldsymbol{\alpha}^e(\mathbf{r}_j) \mathbf{E}(\mathbf{r}_j) + \mathbf{G}_{\text{int}}^{\text{mm}}(\mathbf{r}_i, \mathbf{r}_j) \boldsymbol{\alpha}^m(\mathbf{r}_j) \mathbf{H}(\mathbf{r}_j)] \quad (13)$$

The prime symbol indicates that the case $i = j$ is excluded from the sum because the contribution from the corresponding self-term has been absorbed in our definition of the polarizability tensors (see Eqs. (17) and (18) below). The local fields are linked to the macroscopic fields by

$$\mathbf{E}(\mathbf{r}_i) = \left[\mathbf{I} - \left(\mathbf{G}_{\text{int}}^{\text{ee}}(\mathbf{r}_i, \mathbf{r}_i) + \frac{4\pi}{3} \mathbf{I} \right) \frac{\boldsymbol{\alpha}_0^e(\mathbf{r}_i)}{d^3} \right] \frac{\boldsymbol{\varepsilon}(\mathbf{r}_i) + 2\mathbf{I}}{3} \mathbf{E}_m(\mathbf{r}_i) \quad (14)$$

$$\mathbf{H}(\mathbf{r}_i) = \left[\mathbf{I} - \left(\mathbf{G}_{\text{int}}^{\text{mm}}(\mathbf{r}_i, \mathbf{r}_i) + \frac{4\pi}{3} \mathbf{I} \right) \frac{\boldsymbol{\alpha}_0^m(\mathbf{r}_i)}{d^3} \right] \frac{\boldsymbol{\mu}(\mathbf{r}_i) + 2\mathbf{I}}{3} \mathbf{H}_m(\mathbf{r}_i) \quad (15)$$

with

$$\boldsymbol{\alpha}_0^e(\mathbf{r}_i) = \frac{3d^3}{4\pi} [\boldsymbol{\varepsilon}(\mathbf{r}_i) - \mathbf{I}] [\boldsymbol{\varepsilon}(\mathbf{r}_i) + 2\mathbf{I}]^{-1} \quad \text{and} \quad \boldsymbol{\alpha}_0^m(\mathbf{r}_i) = \frac{3d^3}{4\pi} [\boldsymbol{\mu}(\mathbf{r}_i) - \mathbf{I}] [\boldsymbol{\mu}(\mathbf{r}_i) + 2\mathbf{I}]^{-1} \quad (16)$$

where d is the lattice spacing of the discretization grid. The polarizability tensors used in Eqs. (12)–(13) are then defined as

$$\boldsymbol{\alpha}^e(\mathbf{r}_j) = \boldsymbol{\alpha}_0^e(\mathbf{r}_j) \left[\mathbf{I} - \left(\mathbf{G}_{\text{int}}^{\text{ee}}(\mathbf{r}_i, \mathbf{r}_i) + \frac{4\pi}{3} \mathbf{I} \right) \frac{\boldsymbol{\alpha}_0^e(\mathbf{r}_i)}{d^3} \right]^{-1} \quad (17)$$

$$\boldsymbol{\alpha}^m(\mathbf{r}_j) = \boldsymbol{\alpha}_0^m(\mathbf{r}_j) \left[\mathbf{I} - \left(\mathbf{G}_{\text{int}}^{\text{mm}}(\mathbf{r}_i, \mathbf{r}_i) + \frac{4\pi}{3} \mathbf{I} \right) \frac{\boldsymbol{\alpha}_0^m(\mathbf{r}_i)}{d^3} \right]^{-1} \quad (18)$$

Notice that the standard form of the CDM, including the effect of radiation reaction [2], is obtained by neglecting magnetic effects ($\boldsymbol{\mu} = \mathbf{I}$), making the approximation $\mathbf{G}_{\text{int}}^{\text{ee}}(\mathbf{r}_i, \mathbf{r}_i) \approx (-4\pi/3 + (\frac{2}{3})ik_0^2 d^3) \mathbf{I}$, and assuming that when $i \neq j$ the spatial variation of the field-susceptibility tensor within subunit j can be neglected, i.e. $\mathbf{G}_{\text{int}}(\mathbf{r}_i, \mathbf{r}_j) = \mathbf{G}(\mathbf{r}_i, \mathbf{r}_j)$.

3. Numerical implementation

The local field at all lattice sites is found by solving the linear system comprising Eqs. (12)–(13). This linear system of size of $6N \times 6N$ can be written in matrix form as

$$\left[\begin{pmatrix} \mathbf{I} & \mathbf{0} \\ \mathbf{0} & \mathbf{I} \end{pmatrix} - \begin{pmatrix} \mathbf{G}^{\text{ee}} & \mathbf{G}^{\text{em}} \\ \mathbf{G}^{\text{me}} & \mathbf{G}^{\text{mm}} \end{pmatrix} \begin{pmatrix} \boldsymbol{\alpha}^e & \mathbf{0} \\ \mathbf{0} & \boldsymbol{\alpha}^m \end{pmatrix} \right] \begin{pmatrix} \mathbf{E} \\ \mathbf{H} \end{pmatrix} = \begin{pmatrix} \mathbf{E}_0 \\ \mathbf{H}_0 \end{pmatrix} \quad (19)$$

If the material is isotropic, the matrix containing the polarizabilities is diagonal. Notice that once magnetic effects are included, and even if the material is isotropic, the matrix containing the dyadic tensors is no longer symmetric. As the number of subunits increases the linear system can become large and iterative methods should in general be used to find the self-consistent local fields inside the scatterer. At each iteration we need to compute the product between the matrix which contains the dyadic tensors and the vector which contains the electric and magnetic fields. This product can be computed very efficiently using a fast Fourier transform (FFT) if we use the fact that the tensors actually depend on the relative positions of the source and field points, rather than on their absolute locations: $\mathbf{G}(\mathbf{r}_i, \mathbf{r}_j) = \mathbf{G}(\mathbf{r}_i - \mathbf{r}_j)$ [34,35]. Note that the matrix containing the tensors is only block Toeplitz. To use FFTs we need to embed each Toeplitz block into a circulant matrix of twice the size. Each matrix–vector convolution product, i.e. $\mathbf{G}^{\text{ee}} \boldsymbol{\alpha}^e \mathbf{E}$, $\mathbf{G}^{\text{em}} \boldsymbol{\alpha}^m \mathbf{H}$, $\mathbf{G}^{\text{me}} \boldsymbol{\alpha}^e \mathbf{E}$, and $\mathbf{G}^{\text{mm}} \boldsymbol{\alpha}^m \mathbf{H}$, can then be computed by FFT after the vector is doubled in size and padded with zeros. Because of the symmetry of the field-susceptibility tensors only nine FFTs are required to compute all the elements of the tensors. The result of the original convolution product is then obtained by cropping the result of the cyclic convolution down to the size of the original vector. This method allows us to compute efficiently matrix–vector products. The next step is to choose a “suitable” iterative method to solve the linear system. By suitable we mean an iterative method which leads to a fast convergence of the CDM for the particular problem under study. Although we did not perform an extensive comparison between all the standard iterative methods as Flatau did in Ref. [36], we have noticed that a conjugate gradient approach does not converge very well when both relative permittivity and permeability are different from one. On the other hand, we found that the quasi-minimal-residual (QMR) method of Freund and Nachtigal [37] was more robust, a result in agreement with a recent comparative study of the performance of iterative solvers in the DDA [38]. Incidentally, we point out that when Flatau [36] notes that “QMR is never competitive” it is not because the QMR algorithm is inefficient, rather it is because the QMR code referenced by Flatau, QMR from the parallel iterative method package [39], was not implemented correctly.

In order to study the efficiency of the CDM for material which present both a relative permittivity and relative permeability different from 1, we consider the scattering of light by a sphere with material parameters ε and μ . For this geometry an exact solution can be derived as Mie series [40] and used as a reference.

4. Light scattering by a magnetic sphere

We start by considering the case of an isotropic material with $\text{Re}(\varepsilon) > 1$ and $\text{Re}(\mu) > 1$. We use the CDM to compute the extinction, scattering and absorption cross sections and we extract the relative error compared to Mie theory. In the CDM, the extinction cross section is computed from the forward scattering amplitude using the optical theorem [2] for both electric and magnetic polarizations:

$$C_{\text{ext}} = \frac{4\pi k_0}{|\mathbf{E}_{\text{inc}}|^2} \sum_{i=1}^N \text{Im}[\mathbf{p}(\mathbf{r}_i) \cdot \mathbf{E}_{\text{inc}}^*(\mathbf{r}_i) + \mathbf{m}(\mathbf{r}_i) \cdot \mathbf{H}_{\text{inc}}^*(\mathbf{r}_i)] \quad (20)$$

where $\mathbf{p}(\mathbf{r}_i) = \alpha^e(\mathbf{r}_i)\mathbf{E}(\mathbf{r}_i)$, $\mathbf{m}(\mathbf{r}_i) = \alpha^m(\mathbf{r}_i)\mathbf{H}(\mathbf{r}_i)$ and the asterisk denotes the complex conjugate. The absorption cross section is given by

$$C_{\text{abs}} = \frac{4\pi k_0}{|\mathbf{E}_{\text{inc}}|^2} \sum_{i=1}^N \left[|\mathbf{E}(\mathbf{r}_i)|^2 \left(\text{Im}[\alpha^e(\mathbf{r}_i)] - \frac{2}{3} k_0^3 |\alpha^e(\mathbf{r}_i)|^2 \right) + |\mathbf{H}(\mathbf{r}_i)|^2 \left(\text{Im}[\alpha^m(\mathbf{r}_i)] - \frac{2}{3} k_0^3 |\alpha^m(\mathbf{r}_i)|^2 \right) \right] \quad (21)$$

The scattering cross section can be computed in two ways. The simplest one consists in using $C_{\text{sca}} = C_{\text{ext}} - C_{\text{abs}}$. The second way is based on the computation of the far-field scattered by the object [41]:

$$C_{\text{sca}} = \frac{k_0^2}{|\mathbf{E}_{\text{inc}}|^2} \int \left| \sum_{i=1}^N e^{-ik_0 \mathbf{n} \cdot \mathbf{r}_i} \{ \mathbf{p}(\mathbf{r}_i) - [\mathbf{n} \cdot \mathbf{p}(\mathbf{r}_i)]\mathbf{n} - \mathbf{n} \times \mathbf{m}(\mathbf{r}_i) \} \right|^2 d\Omega \quad (22)$$

where \mathbf{n} is an unit vector in the direction of scattering.

Within the CDM we consider different prescriptions for the polarizabilities: the one based on the Clausius–Mossotti formula with the addition of radiation reaction [2] noted as CR, the prescription by Lakhtakia [32] noted as LA, the prescription introduced by Dungey and Bohren [31], based on the first Mie coefficient, is labeled DB, and finally, our formulation based on the integration of the field-susceptibility tensor over the subunits [3] labeled IT.

We consider a sphere illuminated by a plane wave with wave vector \mathbf{k}_0 . The sphere has material parameters $\varepsilon = \mu = 4 + 2i$ and is discretized into 2176 subunits over a cubic lattice with lattice parameter d . The relative error for the three cross sections are given in Fig. 1. Although the sphere is discretized coarsely, the error remains below 7% over the range of scattering parameters considered (except for the scattering cross section computed as $C_{\text{sca}} = C_{\text{ext}} - C_{\text{abs}}$ in Fig. 1(c) in the long-wavelength regime, which is discussed below). While the different prescriptions for the polarizabilities lead to the same overall evolution of the error with $|\sqrt{\varepsilon\mu}|k_0d$, we see that the error for IT is consistently smaller for $|\sqrt{\varepsilon\mu}|k_0d \ll 1$. However, we also notice that, irrespective of the polarizability used, for all cross sections the error remains non-zero even in the long wavelength or quasi-static approximation $|\sqrt{\varepsilon\mu}|k_0d \rightarrow 0$. We explained this somewhat counterintuitive behavior in Refs. [42,43] (see also [44]). The error in the long-wavelength regime can be interpreted in terms of local-field effects which lead to the dipoles near the surface of the sphere having a different *effective* polarizability from that of the dipoles deeper inside the sphere. Note that this problem would exist even in the limit where the fields are uniform across each cell (e.g. homogeneous sphere placed in a uniform electric field in the electrostatic regime). This is essentially a lattice effect which persists as the discretization grid is reduced and is due to the fact that we are representing what is supposed to be a continuous medium as a discrete collection of volume elements with identical polarizabilities. Notice also that, for small value of $|\sqrt{\varepsilon\mu}|k_0d$, the scattering cross section is computed more efficiently with Eq. (22) than with the simple difference between the extinction and absorption cross sections. If the scattering cross section is computed as the difference between the extinction and absorption cross sections, to avoid round-off errors, one needs to compute these cross sections to a high accuracy which implies a long computation time. In other words, in the long wavelength regime ($d \rightarrow 0$) C_{ext} and C_{abs} are small and close to each other in value. This means that $C_{\text{ext}} - C_{\text{abs}}$ is a very small number. If this number is much smaller than the accuracy with which C_{ext} and C_{abs} have been computed, this may result in a significant relative error on C_{sca} when compared to the Mie result. This explanation is further confirmed by the fact that when we decrease the tolerance of QMR (run a longer computation), the error on $C_{\text{ext}} - C_{\text{abs}}$ becomes comparable to the error on C_{sca} computed directly from the far-fields (Fig. 1d). Therefore, unless the extinction and absorption cross sections are significantly different, C_{sca} is best computed from the scattered far-field, as was pointed out by Draine in Ref. [2].

The effect of the discretization is illustrated in Fig. 2 where we plot the extinction cross section for a sphere of radius $\lambda/5$ (λ being the free-space wavelength of the incident field) versus the value of ε and μ . For the sake of simplicity and in order to plot the result as a single curve we choose $\varepsilon = \mu$. In Fig. 2(a) the Mie calculation shows a number of resonances, including a sharp one for $\varepsilon = \mu \approx 5.2$. Two CDM results are presented alongside the Mie result, for two levels of discretization (8217 dipoles and 65,752 dipoles) and in Fig. 2(b) we zoom in on the sharp resonance and add a new level of discretization with 221,119 dipoles. Quite logically, the finer the discretization, the more accurate the CDM result. In fact, when both ε and μ are positive, the CDM behaves pretty much in the same way as for nonmagnetic material, with the difference that for a given ε , if $\mu \neq 1$ then a finer discretization may be required than in the non-magnetic case.

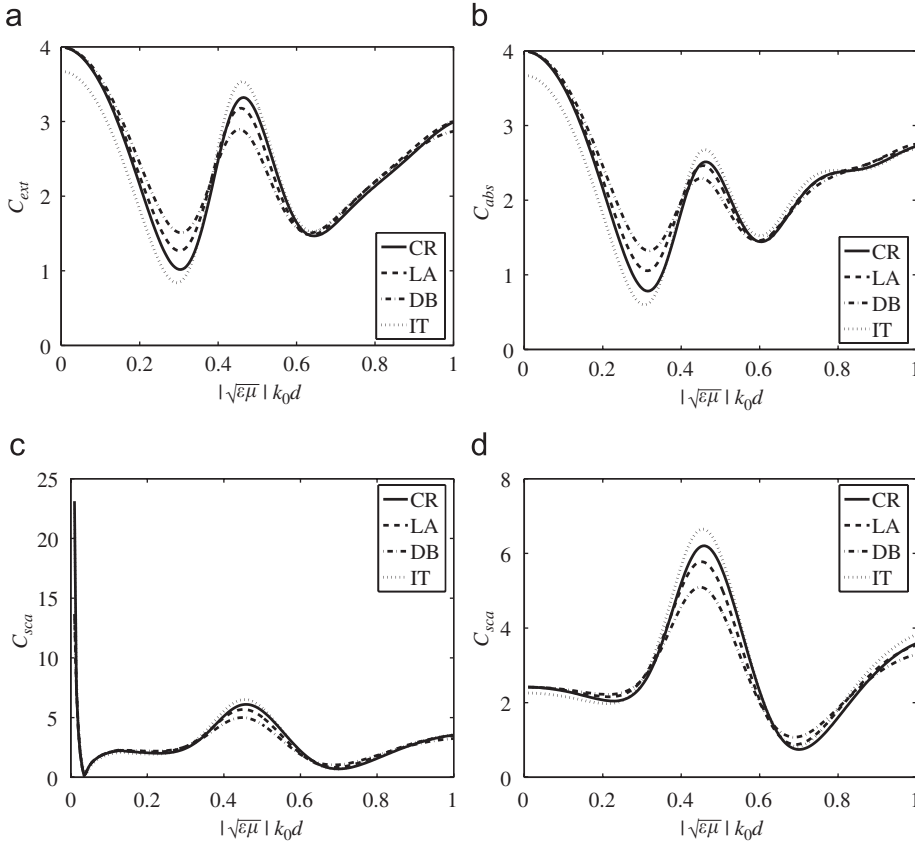


Fig. 1. Relative error in percent for the cross sections compared to Mie theory for a sphere with parameters $\epsilon = \mu = 4 + 2i$, discretized into 2176 dipoles over a cubic lattice with lattice parameter d . (a) Extinction cross section. (b) Absorbing cross section. (c) Scattering cross section obtained from $C_{sca} = C_{ext} - C_{abs}$. (d) Scattering cross section obtained from Eq. (22).

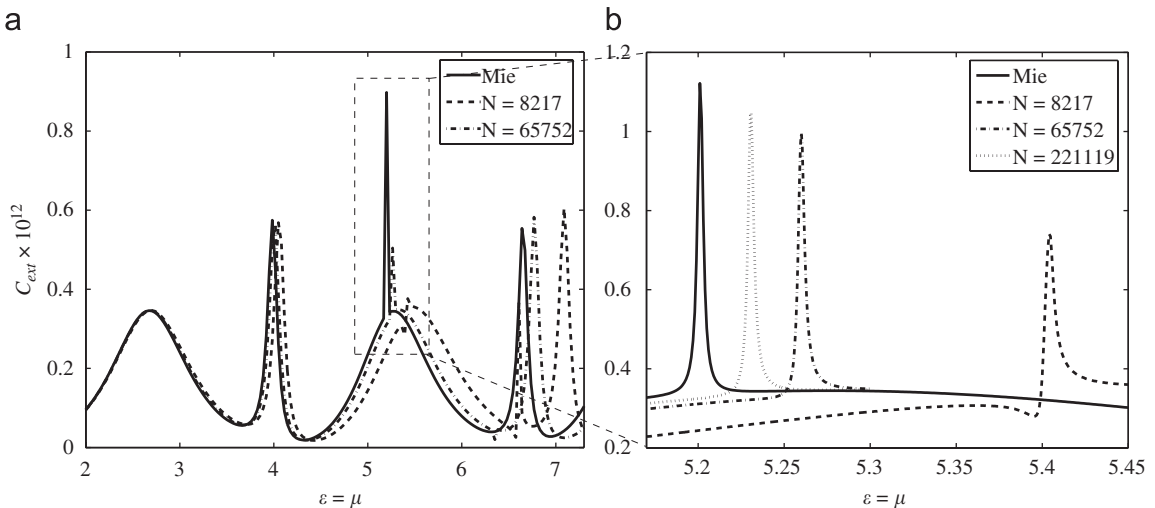


Fig. 2. (a) Extinction cross section versus ϵ and μ for a sphere of radius $\lambda/5$ (size parameter 1.2566) where λ is the free-space wavelength of the incident field. The solid curve is computed using Mie theory whereas the dashed and dashed-dotted curves are computed using the CDM (IT). We consider two levels of discretization (dashed: 8217 dipoles—dashed-dotted: 65,752 dipoles). (b) Zoom on the area represented by the rectangle on panel (a). Beside the curves pertaining to the two levels of discretization shown in panel (a) we also show the curve for $N = 222, 119$ dipoles (dotted curve).

5. Light scattering by a sphere with negative $\text{Re}(\epsilon)$ and $\text{Re}(\mu)$

We now address the case where both $\text{Re}(\epsilon)$ and $\text{Re}(\mu)$ are negative. As we saw previously that the different forms of polarizabilities give similar results, in this section we only consider polarizability (CR) given in Ref. [2]. Fig. 3 shows the extinction cross section, and the relative error of the CDM result compared to Mie, for a sphere with radius $\lambda/10$ and $\text{Re}(\epsilon) = \text{Re}(\mu) = -1$, as a function of the imaginary part of ϵ and μ . We can see that a non-zero imaginary part improves the convergence of the CDM. This is very much the same situation as is encountered in the conventional form of the CDM when dealing with metals with a negative real part of the relative permittivity.

This is illustrated further in Fig. 4 where we consider a sphere with $\text{Re}(\epsilon) = \text{Re}(\mu) = -2$. This situation corresponds to the excitation of the electric and magnetic dipole resonances in the sphere. As far as the electric permittivity is concerned this also corresponds formally to the excitation of the surface plasmon mode of a small metallic sphere. For the metallic sphere it is well known that the convergence of the CDM around the plasmon resonance is improved by the addition of a damping term. Fig. 4 shows a similar trend for a negative-refraction material with $\text{Re}(\epsilon) = \text{Re}(\mu) = -2$. Because these values of $\text{Re}(\epsilon)$ and $\text{Re}(\mu)$ correspond to poles of the Clausius–Mossotti polarizabilities, the relative error of the CDM compared to Mie decreases slower with the imaginary part of the optical constants than in the case where $\text{Re}(\epsilon) = \text{Re}(\mu) = -1$. As a general rule, when using the CDM to model a negative-refraction material similar rules to those used with metals should be used. Unless the damping terms (imaginary parts of the optical constants) are significant, a fine discretization should be used. Clearly, the convergence problems will occur preferentially when $\text{Re}(\epsilon)$ and/or $\text{Re}(\mu)$ are equal to -2 as shown in Fig. 5 where we plot the value of the extinction cross section and its relative error compared to Mie theory, as a function of the real part of the optical constants, for a sphere of radius $\lambda/20$. We consider two values of the absorption. In Fig. 5(a), we have $\text{Im}(\epsilon) = \text{Im}(\mu) = 0.1$, while the absorption is increased to $\text{Im}(\epsilon) = \text{Im}(\mu) = 1$ in Fig. 5(b). As we can see in Fig. 5(a), when $\text{Re}(\epsilon) = \text{Re}(\mu) \approx -2$ and the absorption is weak, increasing the number of dipoles certainly helps a little, however, the

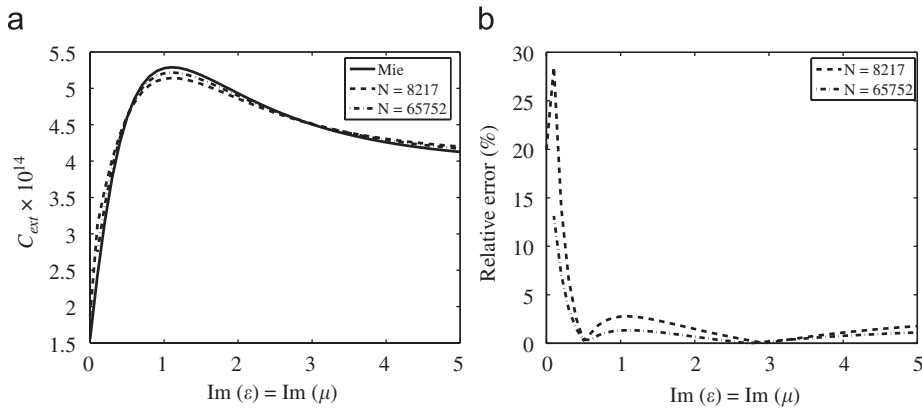


Fig. 3. Sphere with radius $\lambda/10$ (size parameter 0.6283) and $\text{Re}(\epsilon) = \text{Re}(\mu) = -1$. Extinction cross section (a) and relative error (b), versus the imaginary part of ϵ and μ .

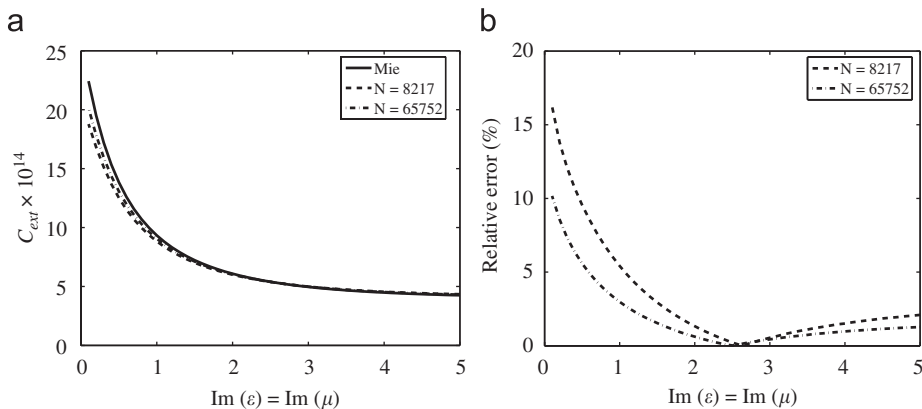


Fig. 4. Sphere with radius $\lambda/10$ (size parameter 0.6283) and $\text{Re}(\epsilon) = \text{Re}(\mu) = -2$. Extinction cross section (a) and relative error compared to Mie theory (b), versus the imaginary part of ϵ and μ .

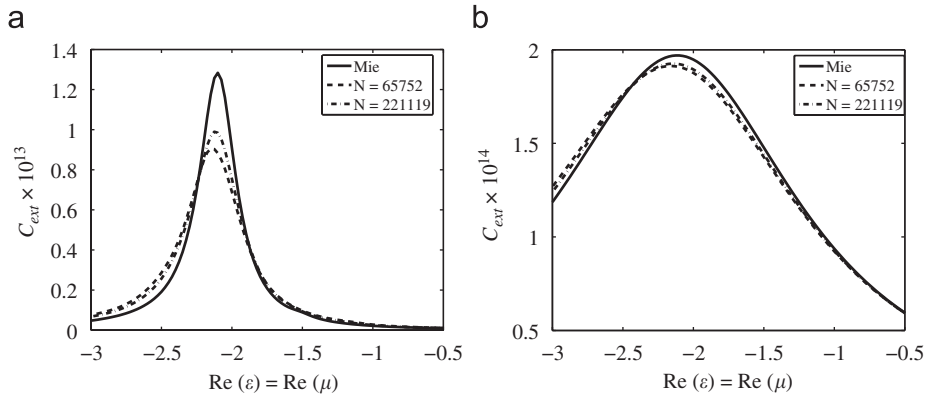


Fig. 5. Extinction cross section versus the real part of ε and μ for a sphere with radius $\lambda/20$ (size parameter 0.3142) and $\text{Re}(\varepsilon) = \text{Re}(\mu) < 0$, for two values of the imaginary part of ε and μ : (a) $\text{Im}(\varepsilon) = \text{Im}(\mu) = 0.1$ and (b) $\text{Im}(\varepsilon) = \text{Im}(\mu) = 1$.

convergence is very slow. On the other hand, the presence of a stronger absorption (Fig. 5(b)) ensures that the CDM computation is reasonably accurate even at a modest level of discretization.

6. Conclusion

We have presented a formulation of the CDM that can be used to study the scattering of light by an arbitrary object with an arbitrary dielectric permittivity and magnetic permeability. We have shown that while magnetic material can be treated in pretty much the same fashion as non-magnetic material, negative-refraction material demand greater care. Indeed, as the CDM treats arbitrary objects as a collection of dipoles (electric and magnetic), whenever the real part of the permittivity and/or the permeability is close to -2 , strong dipole resonances occur. In this case, the weaker the material absorption, the finer the discretization should be, however, one should expect a very slow convergence. Finally, let us note that along the lines of the present derivation, the previous studies based on the CDM (spontaneous emission, optical forces, etc.) can be extended to treat magnetic and negative-refraction materials.

References

- [1] Purcell EM, Pennypacker CR. Scattering and absorption of light by nonspherical dielectric grains. *Astrophys J* 1973;186:705–14.
- [2] Draine BT. The discrete-dipole approximation and its application to interstellar graphite grains. *Astrophys J* 1988;333:848–72.
- [3] Chaumet PC, Sentenac A, Rahmani A. Coupled dipole method for scatterers with large permittivity. *Phys Rev E* 2004;70:036606–6.
- [4] Rahmani A, Chaumet PC, de Fornel F. Environment-induced modification of spontaneous emission: single-molecule near-field probe. *Phys Rev A* 2001;63:023819–911.
- [5] Lumme K, Rahola J. Light scattering by porous dust particles in the discrete-dipole approximation. *Astrophys J* 1994;425:653–67.
- [6] Kimura H. Light-scattering properties of fractal aggregates: numerical calculations by a superposition technique and the discrete-dipole approximation. *JQSRT* 2001;70:581–94.
- [7] Moreno F, Vilaplana R, Muñoz O, Molina A, Guirado D. The scattering matrix for size distributions of irregular particles: an application to an olivine sample. *JQSRT* 2006;100:277–87.
- [8] Zubko E, Shkuratov Y, Kiselev NN, Videen G. DDA simulations of light scattering by small irregular particles with various structure. *JQSRT* 2006;101:416–34.
- [9] Muinonen K, Zubko E, Tynnela J, Shkuratov Y, Videen G. Light scattering by Gaussian random particles with discrete-dipole approximation. *JQSRT* 2007;106:360–77.
- [10] Zubko E, Muinonen K, Shkuratov Y, Videen G, Nousiainen T. Scattering of light by roughened Gaussian random particles. *JQSRT* 2007;106:604–15.
- [11] Zubko E, Shkuratov Y, Mishchenko M, Videen G. Light scattering in a finite multi-particle system. *JQSRT* 2008;109:2195–206.
- [12] Yurkin MA, Hoekstra AG. The discrete dipole approximation: an overview and recent developments. *JQSRT* 2007;106:558–89.
- [13] Rahmani A, Bryant GW. Spontaneous emission in microcavity electrodynamics. *Phys Rev A* 2002;65:033817–912.
- [14] Bordas F, Louvion N, Callard S, Chaumet PC, Rahmani A. Coupled dipole method for radiation dynamics in finite photonic crystal structures. *Phys Rev E* 2006;73:056601.
- [15] Draine BT, Weingartner JC. Radiative torques on interstellar grains: I. Superthermal spinup. *Astrophys J* 1996;470:551–65.
- [16] Chaumet PC, Nieto-Vesperinas M. Coupled dipole method determination of the electromagnetic force on a particle over a flat dielectric substrate. *Phys Rev B* 2000;61:14119–27.
- [17] Chaumet PC, Billaudeau C. Coupled dipole method to compute optical torque: application to a micropopler. *J Appl Phys* 2007;101:023106–6.
- [18] Chaumet PC, Nieto-Vesperinas M. Optical binding of particles with or without the presence of a flat dielectric surface. *Phys Rev B* 2001;64:035422–7.
- [19] Chaumet PC, Rahmani A, Nieto-Vesperinas M. Optical trapping and manipulation of nano-object with an apertureless probe. *Phys Rev Lett* 2002;88:123601–4.
- [20] Chaumet PC, Rahmani A, Nieto-Vesperinas M. Selective nanomanipulation using optical forces. *Phys Rev B* 2002;66:195405–11.
- [21] Rahmani A, Chaumet PC. Optical trapping near a photonic crystal. *Opt Express* 2006;14:6353–8.
- [22] Chaumet PC, Rahmani A, Nieto-Vesperinas M. Local-field enhancement in an optical force metallic nanotrap: application to single-molecule spectroscopy. *Appl Opt* 2006;45:5185–90.
- [23] Sentenac A, Chaumet PC, Belkebir K. Beyond the Rayleigh criterion: grating assisted far-field optical diffraction tomography. *Phys Rev Lett* 2006;97:243901.
- [24] Yurkin MA, Hoekstra AG, Brock RS, Lu JQ. Systematic comparison of the discrete dipole approximation and the finite difference time domain method for large dielectric scatterers. *Opt Express* 2007;15:17902–11.

- [25] Yurkin MA, Maltsev VP, Hoekstra AG. The discrete dipole approximation for simulation of light scattering by particles much larger than the wavelength. *JQSRT* 2007;106:546–57.
- [26] Mulholland GW, Bohren CF, Fuller KA. Light scattering by agglomerates coupled electric and magnetic dipole method. *Langmuir* 1996;10(8):2533–46.
- [27] Lemaire T. Coupled-multipole formulation for the treatment of electromagnetic scattering by a small dielectric particle of arbitrary shape. *J Opt Soc Am A* 1997;14(2):470–4.
- [28] Lakhtakia A. General theory of the Purcell–Pennypacker scattering approach and its extension to bianisotropic scatterers. *Astrophys J* 1992;394:494–9.
- [29] You Y, Kattawar GW, Zhai P-W, Yang P. Zero-backscatter cloak for aspherical particles using a generalized dda formalism. *Opt Express* 2008;16:2068–79.
- [30] Agarwal GS. Quantum electrodynamics in the presence of dielectrics and conductors. I Electromagnetic-field response functions and black-body fluctuations in finite geometry. *Phys Rev A* 1975;11:230–42.
- [31] Dungey CE, Bohren CF. Light scattering by nonspherical particles: a refinement to the coupled-dipole method. *J Opt Soc Am A* 1991;8(1):81–7.
- [32] Lakhtakia A. Strong and weak forms of the method of moments and the coupled dipole method for scattering of time-harmonic electromagnetics fields. *Int J Mod Phys C* 1992;3:583–603.
- [33] Draine BT, Goodman J. Beyond Clausius–Mossotti: wave propagation on a polarizable point lattice and the discrete dipole approximation. *Astrophys J* 1993;405:685–97.
- [34] Goodman JJ, Draine BT, Flatau PJ. Application of fast-Fourier-transform techniques to the discrete-dipole approximation. *Opt Lett* 1991;16:1198–200.
- [35] Draine BT, Flatau PJ. Discrete-dipole approximation for scattering calculations. *J Opt Soc Am A* 1994;11:1491–9.
- [36] Flatau PJ. Improvements in the discrete-dipole approximation method of computing scattering and absorption. *Opt Lett* 1997;22:1205–7.
- [37] Freund RW, Nachtigal NM. QMR—a quasi-minimal residual method for non-Hermitian linear-systems. *Numer Math* 1991;60(3):315–39.
- [38] Fan ZH, Wang DX, Chen RS, Yung EKN. The application of iterative solvers in discrete dipole approximation method for computing electromagnetic scattering. *Microwave Opt Technol Lett* 2006;48:1741–6.
- [39] Da Cunha RD, Hopkins T. The parallel iterative methods (PIM) package for the solution of systems of linear equations on parallel computers. *Appl Numer Math* 1995;19:33–50.
- [40] Garcia-Camara B, Moreno F, Gonzalez F, Saiz JM, Videen G. Light scattering resonances in small particles with electric and magnetic properties. *J Opt Soc Am A* 2008;25(2):327–34.
- [41] Jackson JD. *Classical electrodynamics*. 2nd ed. New York: Wiley; 1975.
- [42] Rahmani A, Chaumet PC, Bryant GW. Coupled dipole method with an exact long-wavelength limit and improved accuracy at finite frequencies. *Opt Lett* 2002;27(23):2118–20.
- [43] Rahmani A, Chaumet PC, Bryant GW. On the importance of local-field corrections for polarizable particles on a finite lattice: application to the discrete dipole approximation. *Astrophys J* 2004;607:873–8.
- [44] Collinge MJ, Draine BT. Discrete dipole approximation with polarizabilities that account for both finite wavelength and target geometry. *J Opt Soc Am A* 2004;21:2023–8.